Monthly Notices
of the
ROYAL ASTRONOMICAL SOCIETY

Mon. Not. R. Astron. Soc. **400,** 168–175 (2009) doi:10.1111/j.1365-2966.2009.15468.x

The X-ray properties of the energetic pulsar PSR J1838−0655

Lupin Chun-Che Lin,[1⋆] Jumpei Takata,[2] Chorng-Yuan Hwang[1] and Jau-Shian Liang[3]

[1]*Graduate Institute of Astronomy, National Central University, Jhongli 32001, Taiwan*
[2]*Theoretical Institute for Advanced Research in Astrophysics, National Tsing Hua University, Hsinchu 30013, Taiwan*
[3]*Department of Physics, National Tsing Hua University, Hsinchu 30013, Taiwan*

Accepted 2009 July 30. Received 2009 July 30; in original form 2009 June 23

ABSTRACT

We present and interpret several new X-ray features of the X-ray pulsar PSR J1838−0655. The X-ray data are obtained from the archival data of *Chandra*, *RXTE* and *Suzaku*. We combine all these X-ray data and fit the spectra with different models. We find that the joint spectra are difficult to fit with a single power law; a broken power-law model with a break at around 6.5 keV can improve the fit significantly. The photon index changes from $\Gamma = 1.0$ (below 6.5 keV) to 1.5 (above 6.5 keV); this indicates a softer spectral behaviour at hard X-rays. The X-ray flux at 2–20 keV is found to be 1.6×10^{-11} erg cm^{-2} s^{-1}. The conversion efficiency from the spin-down luminosity is ∼0.9 per cent at 0.8–10 keV, which is much higher than that (∼10^{-3} to 10^{-4} per cent) of the pulsars that show similar timing properties. We discuss non-thermal radiation mechanisms for the observed high X-ray conversion efficiency and find that emission from the magnetosphere of a greatly inclined rotator is the most favourable interpretation for the conversion rate and the pulse profiles at X-ray bands. A line feature close to 6.65 keV is also detected in the spectra of *Suzaku*/X-ray imaging spectrometer; it might be the Kα emission of highly ionized Fe surrounding the pulsar.

Key words: line: identification – radiation mechanisms: general – pulsars: general – gamma-rays: observations – X-rays: general.

1 INTRODUCTION

PSR J1838−0655 is an X-ray pulsar that was recently discovered. This X-ray source was first catalogued by *Einstein* imaging proportional counter (IPC) in the Galactic plane survey (1E 1835.3–0658; Hertz & Grindlay 1988). *ASCA* found that this source, which was named as AX J1838.0−0655 according to the nomenclature of *ASCA*, is located at the southern edge of the supernova remnant SNR G25.5+0.0 (Bamba et al. 2003). Sugizaki et al. (2001) suggested AX J1838.0−0655 to be a variable source; however, Bamba et al. (2003) and Malizia et al. (2005) reanalysed the *ASCA* data and obtained a steady flux for this source. AX J1838.0−0655 was finally identified as an X-ray pulsar because of the discovery of the spin period at 70.5 ms using *RXTE* data (Gotthelf & Halpern 2008).

AX J1838.0−0655 is a bright X-ray source with a hard ($\Gamma = 0.8 \pm 0.4$) non-thermal spectrum (Bamba et al. 2003). The observed fluxes of *ASCA* (0.7–10 keV; Bamba et al. 2003), *Chandra* (2–10 keV; Gotthelf & Halpern 2008) and *Suzaku* (0.4–10 keV; Anada et al. 2009) are ∼ 0.88, 1.1 and 1.32×10^{-11} erg cm^{-2} s^{-1}, respectively. The flux in 2–6 keV of the *ASCA* spectrum (∼0.4×10^{-11}erg cm^{-2} s^{-1}) was different from that of the *EXOSAT* source GPS 1835–070 (∼6.3×10^{-11} erg cm^{-2} s^{-1}), which was an X-ray source discovered at the positional uncertainty of AX J1838.0−0655 with the medium-energy proportional counters on *EXOSAT* (Warwick et al. 1988). However, the variability of the point-source flux between the two investigations of *EXOSAT* and *ASCA* might be caused by the contamination from nearby sources in the detection of *EXOSAT*. The IBIS/ISGRI on board *INTEGRAL* has also detected this X-ray source at hard X-rays/γ-rays. (Bassani et al. 2004; Bird et al. 2004).

A single absorbed power law usually gave a good fit to the X-ray spectra of PSR J1838−0655, but the photon indices might vary at different wavebands. A single power law with a photon index of $\Gamma = 1.5 \pm 0.2$ and a column density of $N_{\rm H} = (6.7 \pm 1.3) \times 10^{22}$ cm^{-2} provided a good fit to the composite spectra from 1 to 300 keV generated by *ASCA/INTEGRAL* (Malizia et al. 2005). At low-energy wavebands, the observations of *ASCA*/Gas Imaging Spectrometer (GIS) and *Chandra*/Advanced CCD Imaging Spectrometer (ACIS) indicated a harder spectrum with $\Gamma = 0.8 \pm 0.4$ (0.7–10 keV) and 0.5 ± 0.2 (2–10 keV) (Sugizaki et al. 2001; Gotthelf & Halpern 2008). However, we note that the photon indices derived from *Suzaku*/X-ray imaging spectrometer (XIS) (Anada et al. 2009 $\Gamma = 1.27 \pm 0.11$) and *Swift*/XRT (Landi et al. 2006, $\Gamma = 1.86^{+0.69}_{-0.46}$) were significantly softer than the results of *ASCA*/GIS and *Chandra*/ACIS at similar wavebands. On the other hand, the results of *Beppo-SAX*/Phoswich Detection System (PDS), *INTEGRAL*/ISGRI and *Suzaku*/hard X-ray detector (HXD) showed much softer spectra

⋆E-mail: lupin@crab0.astr.nthu.edu.tw

at high-energy wavebands with Γ around 2.5 to 1.6 (Malizia et al. 2004, 2005; Anada et al. 2009). Furthermore, Gotthelf & Halpern (2008) and Anada et al. (2009) claimed that the spectrum of PSR J1838−0655 became steepened at around 8–15 keV; the truth and the origin of the spectral break or steepening are still unclear. Besides, we note that the detected X-ray emission might contain emission from the pulsar wind nebula (PWN) (Γ = 1.1–2.0 in 2–10 keV, Gotthelf & Halpern 2008) and/or emission from the supernova remnant.

The high-energy nature of AX J1838.0−0655 has caught more attention when Aharonian et al. (2005) showed a possible connection between AX J1838.0−0655 and a high-energy TeV source, HESS J1837–069. Aharonian et al. (2006b) indicated that HESS J1837–069 might be associated with supernova remnants or PWNe; and this suggested that AX J1838.0−0655 might be a pulsar candidate before its pulsation was confirmed. Furthermore, the non-thermal spectral behaviour with a photon index similar to the general pulsars (Γ ∼ 0.5– 2.5) and the large flux ratio between the X-ray and optical band, $F_{0.4-10\mathrm{keV}}/F_{1\mathrm{eV}}$ (Gotthelf & Halpern 2008; this value is ∼100–1000 for the Vela pulsar) also gave supporting evidence indicating this X-ray source to be a pulsar.

No radio counterpart of the X-ray pulsar PSR J1838−0655 has been detected yet. If HESS J1837−069 is the TeV counterpart of the X-ray pulsar, the radio brightness of HESS J1837−069 will be extremely faint compared with other known TeV sources. Besides, unlike the Geminga pulsar, PSR J1838−0655 has no detectable γ-rays from hundreds MeV to hundreds GeV (Hartman 1999; Abdo 2009).

The energy-conversion efficiency of PSR J1838−0655 is very unique compared with other known X-ray pulsars with similar properties. For example, the characteristic age, the surface dipole magnetic field and the spin-down luminosity of PSR J1838−0655 are all very similar to those of PSRs B0833–45 (the Vela) and B1706–44; however, the energy-conversion efficiency of PSR J1838−0655 is about two to three orders of magnitude higher than those of PSRs B0833–45 and B1706–44 as inferred from the observed X-ray emission in 0.8–10 keV. Therefore, PSR J1838−0655 provides a unique opportunity to investigate the energy-conversion mechanism and to understand the nature of the X-ray emission of pulsars.

To understand the puzzling properties of the X-ray emission of PSR J1838−0655, we re-examine the X-ray spectral behaviour of this pulsar using *Chandra*, *RXTE* and *Suzaku* archives. We propose possible mechanisms to explain the observed X-ray spectrum and the high energy conversion efficiency of PSR J1838−0655. We also marginally detect a line feature at around 6.65 keV, which might be Kα emission of highly ionized Fe on or around the surface of the pulsar.

2 OBSERVATIONS AND DATA ANALYSIS

To study the emission mechanisms of PSR J1838−0658, we reanalysed its spectral and temporal behaviours using the X-ray archives of *Chandra*, *RXTE* and *Suzaku*.

2.1 *Chandra* data

The *Chandra* data were observed on 2006 August 19 using the advanced CCD imaging spectrometer operating in the timed exposure (TE)/VFAINT mode with an exposure time of 20 ks. The same data have been analysed by Gotthelf & Halpern (2008). The data reduction and spectral analysis were performed using standard procedures with the X-ray packages of CIAO (ver. 3.4.1.1), CALDB 4.1.1 and XSPEC (ver. 12.4.0). We followed Gotthelf & Halpern (2008) in selecting the regions for the pulsar, the PWN and the background. The spectra of PSR J1838−0655 and the PWN are grouped to have at least 50 counts for each spectral bin.

2.2 *RXTE* data

The *RXTE* data were observed from 2008 February 17 to March 5 using the Proportional Counter Array (PCA; 2–60 keV). The same data set has been used by Gotthelf & Halpern (2008) to determine the period and period derivative of PSR J1838−0655. The time resolution of the data set is very high (1 μs) and can provide a proper detection of the pulsed spectra of the pulsars. We performed the standard data-reduction procedures with the FTOOLS (ver 6.5) of HEASOFT (ver. 6.5.1) using the latest PCA calibration files (20090313). The events that we used for spectral analysis were restricted to Good Xenon and Good Time Interval (GTI). The total exposures of GTIs are 12.9 ks for Proportional Counter Unit (PCU) 0, 9.3 ks for PCU 1, 31.5 ks for PCU 2 , 4.1 ks for PCU 3 and 8.2 ks for PCU 4. We also set the energy boundary of photons at 2–20 keV.

After getting the final products, we performed the Solar system barycentric time correction using 'faxbary' at (J2000) RA = 279.°513, Dec. = −6.°926 to produce an event time list for the following analysis. According to the timing ephemeris derived by Gotthelf & Halpern (2008), we set the period as 70.498 243 97 ms and the period derivative 4.925×10^{-14} s s^{-1} at the epoch of 54522.000 696 574 MJD and folded the *RXTE* data to produce the pulsed profile of PSR J1838−0655 as shown in Fig. 1.

To generate the pulsed spectrum, we assumed the unpulsed emission to be the background. We divided the data into 'on-peak' and 'off-peak' emission depending on their pulsed phase. The response of each PCU was produced by the Perl script of 'PCARSP' and then combined by the task of 'ADDRMF' with the weighting depending on the relative exposures. The pulsed spectrum was then obtained by subtracting the off-peak emission from the on-peak emission.

2.3 *Suzaku* data

The *Suzaku* observations of PSR J1838−0655 were carried out in 2007 March. The archival data contain observational results of the XIS and the non-imaging HXD. The data sets have been analysed by Anada et al. (2009).

2.3.1 XIS

The *Suzaku*/XIS observations of PSR J1838−0655 have a total exposure of 42.2 ks. The data were observed in the normal mode without window option and the pixels on the CCD were read out every 8 s. The 42.2 ks exposure of XIS observation was divided into two editing modes of 5 × 5 and 3 × 3 with 14.9 and 27.3 ks, respectively.

The selection of source area for the *Suzaku*/XIS data in our analysis is slightly different from that of Anada et al. (2009). Because PSR J1838−0655 is contaminated by some nearby sources, which can marginally be resolved in the XIS image (e.g. GPSR5 25.252–0.139; Gotthelf & Halpern 2008), we extracted the spectra of PSR J1838−0655 only within 1.5 arcmin circular regions centred at (J2000) RA = $18^{\mathrm{h}}38^{\mathrm{m}}03^{\mathrm{s}}.13$, Dec. = $-06^{\circ}55'33''.4$ instead of the regular adoption of 3 arcsec circular region for a point source. Our selection still contains ∼70 per cent of the total energy for a point source. We extracted the background of the pulsar from a concentric

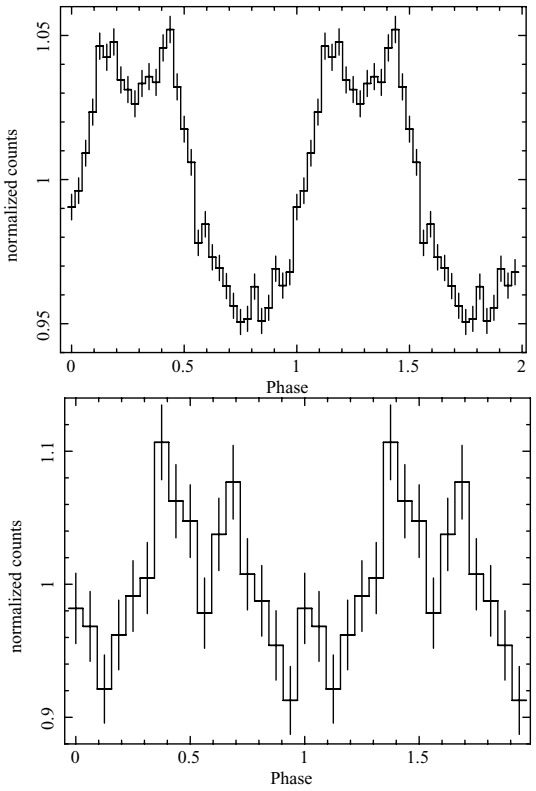

Figure 1. (a) The upper panel shows pulse profile in 2–20 keV folded by 32 bins with the period of 70.498 243 97 ms and the period derivative of 4.925×10^{-14} using 8 *RXTE*/PCA data from 2008 February 17 to March 5. The time zero (t_0) of the profile was set at the epoch of 54522.000 696 574 MJD. (b) The lower panel shows the pulse profile in 10–60 keV folded by 16 bins with the period of 70.496 725 ms using *Suzaku*/HXD–PIN data of 2007 March 5. The time zero of the profile was set at the start of GTI (54164.533 942 70 MJD). Both (a) and (b) are divided into two groups to represent the pulsed phase and unpulsed phase. We determined the pulsed phase (on-peak emission) as 0.625 cycle. The pulsed phase of (a) starts from 1st to 20th bin of 32 bins and that of (b) starts from 4th to 14th bin of 16 bins. The plot of the counts are normalized to the average photons in each bin.

annulus of radii $2.5 < r \leq 3.5$ arcmin centred at the pulsar position and set the energy boundary to be 0.5–10 keV. The extracted spectra comprise 2935 counts for XIS 0, 2180 counts for XIS 1 and 3427 counts for XIS 3 after subtracting the background.

The XIS data reduction and spectral analysis were executed using XSELECT (ver. 2.4a) of HEASOFT (ver. 6.5.1) and XSPEC (ver. 12.4.0) with the latest *Suzaku*/XIS calibration files (20090203). We generated the response matrix (rmf) and auxiliary response (arf) files with the HEASOFT command of 'XISRMFGEN' and 'XISSIMARFGEN'. The spectra are produced with each channel containing at least 50 counts. A cross-calibration term was included to correct the difference among three XIS spectra at 0.5–10 keV.

2.3.2 HXD

The *Suzaku*/HXD observations of PSR J1838−0655 have a total exposure of 37.7 ks and offer a time resolution of 6 μs for pulsed detection. However, the spectrum of the *Suzaku*/gadolinium silicon oxide scintillation counters data is not good enough for statistical analysis, we thus only reduced and analysed the pulsed spectral data obtained from the HXD–positive intrinsic negative (PIN) silicon diodes. We performed the data reduction and spectral analysis procedures of the PIN data using XSELECT (ver. 2.4a), FTOOLS (ver 6.5) of HEASOFT (ver. 6.5.1) and XSPEC (ver. 12.4.0) with the latest HXD calibration files (20090203). The events were restricted to the effective energy range (10–60 keV) of the PIN detector. We also applied Solar system barycentric time correction with the task 'AEBARYCEN' at (J2000) RA = 279.°513, Dec. = −6.°926 in order to produce and analyse the pulsation of PSR J1838−0655. Based on the timing ephemeris derived by Gotthelf & Halpern (2008), we set a trial period of 70.496725 ms at epoch MJD 54164.98049 (the mid-point of this *Suzaku*/HXD observation).

The hard X-ray spectrum obtained by subtracting the non-X-ray background and cosmic X-ray background was divided into two groups of phase cycles to represent the 'on-peak' and 'off-peak' emission. The pulsed spectral data were obtained by subtracting the off-peak emission from the on-peak emission and rebinned to ensure that the photons in each spectral channel are larger than 50 after subtracting the unpulsed background. The pulsed photons of PSR J1838−0655 above 50 keV are very few in the data and are thus ignored in spectral analysis.

3 RESULTS

Table 1 shows the results of our spectral analysis for *Chandra*, *RXTE* and *Suzaku* observations. We also show the results of previous analysis in Table 1 for comparisons. Our results are consistent with previous analyses; however, some significant discoveries are found in our work. First, we identify a spectral break at 6.5 ± 1.0 keV, which is roughly consistent with the previous claim of Gotthelf & Halpern (2008) and Anada et al. (2009) that the spectrum steepens at around 8–15 keV. Secondly, we find a line feature around 6.4 keV in the spectra of *Suzaku*/XIS.

We have applied a simultaneous fit to a composite spectrum of PSR J1838−0655 (Fig. 2). We included the spectra of ACIS/*Chandra*, PCA/*RXTE* and HXD/*Suzaku*; all these spectra are believed to be dominated by the pulsed phases. To account for the cross-calibration mismatch between each instrument, we also introduced a constant to this fit. In order to compare with the joint spectrum of *ASCA/INTEGRAL* data (Malizia et al. 2005), we have fixed the column density to 6.7×10^{22} cm^{-2} in our analysis. A single absorbed power-law model for the composite spectrum has a power-law index of $\Gamma = 1.2 \pm 0.1$ with $\chi^2_\nu = 1.35$ for 91 degrees of freedom (d.o.f.). The statistics does not improve even if we set the absorbed column density as the free parameter to fit the spectra.

A broken power-law model can obviously improve the fit of the joint spectrum and the additional power-law component is significant at more than 99 per cent via an F-test. The power-law indices change from $1.0^{+0.1}_{-0.2}$ to $1.5^{+0.3}_{-0.2}$ with the broken energy at $6.5^{+1.0}_{-1.0}$ KeV. The statistics have significantly improved to $\chi^2_\mu = 1.20$ for 89 d.o.f. We note that a similar spectral break has been discovered in the Crab pulsar (Kuiper et al. 2001).

To check whether the broken power law is caused by the instrumental responses of different observations, we have also applied the power-law models to different energy bands of the *RXTE* data to examine the variation of the photon indices of the pulsed spectrum. Originally, no significant variation of the photon index was found between the energy domains less than 10 keV and larger than 10 keV ($\Gamma \sim 1.0$–1.1). However, we note that both photon indices are flatter than that of the total spectrum. We thus examine the photon index of the spectrum at the energy of 5–15 keV and find the photon index $\Gamma \sim 1.4$. This suggests that there is a spectral break

Table 1. Single power-law spectra for AX J1838.0−0655/PSR J1838−0655 detected by different X-ray observations.

Instrument	Energy range (keV)	Photon index (Γ)	Column density (10^{22} cm^{-2})	Unabsorbed flux (10^{-11} erg cm^{-2} s^{-1})	References
Einstein/IPC	0.2–3.5	–	–	0.014[a]	Hertz & Grindlay (1988)
ASCA/GIS	0.7–10.0	0.8 (0.4–1.2)	4.0 (2.8–5.7)	1.1	Sugizaki et al. (2001)
Beppo-SAX/PDS	20–100	2.5 (2.2–2.8)	–	3.6	Malizia et al. (2004)
INTEGRAL/ISGRI	20–300	1.66 (1.43–1.89)	–	9.0	Malizia et al. (2005)
Swift/XRT	0.2–8.5	1.86 (1.4–2.55)	5.54 (3.73–8.37)	1.13[b]	Landi et al. (2006)
Chandra/ACIS	2–10	0.5 (0.3–0.7)	4.5 (3.7–5.2)	0.88	Gotthelf & Halpern (2008)
		0.5 (0.2–0.7)	4.1 (2.7–5.5)	0.86	This work
RXTE/PCA[c]	2–20	1.2 (1.1–1.3)	4.5 (fixed)	0.9[b]	Gotthelf & Halpern (2008)
		1.3 (1.2–1.4)	4.1 (fixed)	0.92[b]	This work
Suzaku/XIS	0.4–10	1.27 (1.16–1.38)	5.4 (4.9–5.9)	1.32	Anada et al. (2009)
	0.5–10	1.37 (1.28–1.50)	6.0 (5.6–6.5)	1.26	This work
Suzaku/HXD[c]	12–50	2.0 (1.1–3.0)	–	1.84	Anada et al. (2009)
	10–50	2.0 (0.9–3.3)	6.7 (fixed)	1.9	This work

Note. The errors are set in 90 per cent confidence interval throughout.
[a]X-ray flux in IPC counts s^{-1}. [b]Indicated in 2–10 keV. [c]Only the pulsed spectra were calculated.

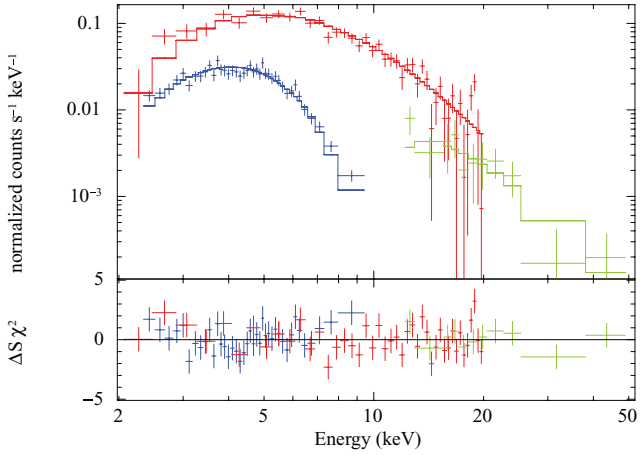

Figure 2. Cross-calibration fit of the joint spectra (blue: *Chandra*/ACIS; red: *RXTE*/PCA and green: *Suzaku*/HXD–PIN; the vertical axis of the *RXTE* spectrum is referred to only one PCU). We applied a broken power law with a change of the slope from 1.0 to 1.5 and a break energy at 6.5 keV to get the best spectral fit. The bottom panel shows the residuals in terms of σs with error bars of size 1.

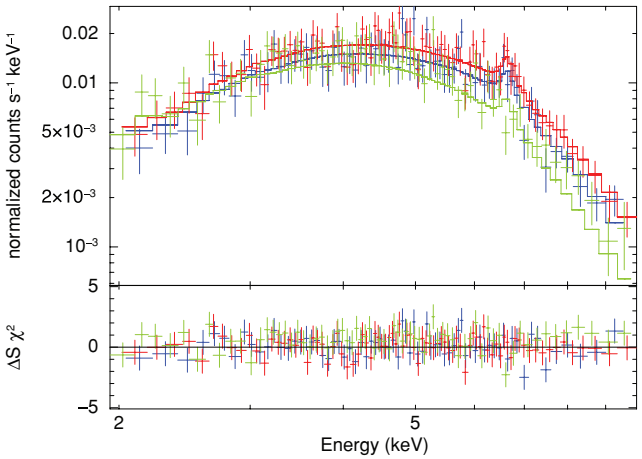

Figure 3. Spectra of three XIS detectors from 2–10 keV (Blue: XIS 0; Green: XIS 1 and Red: XIS 3). Each spectral channel has at least 30 counts. In the simultaneous fitting for the spectra of two FI XIS detectors, we proposed the absorbed power law and Lorentz line profile to fit the data sets, and the line emission was marginally detected close to 6.4 keV. The bottom panel shows the residuals in terms of σs with error bars of size 1.

at around 10 keV, and the break is not caused by the uncertainty of the response functions among the different instruments.

We also note that the *RXTE* spectrum is very different from the *Chandra* one, which shows a much flatter photon index ($\Gamma \sim 0.5$). We note that the time resolution for the *Chandra* TE mode data is only about 3.2 s, and it is not adequate to get the pulsed spectrum from timing analysis. However, if the unpulsed emission is mainly contributed by the surrounding ionized cloud, the pulsed spectrum can roughly be obtained by considering the spectrum of its PWN as the background of the pulsar. The PWN spectrum can be well fitted with a power law with a photon index of $\Gamma \sim 1.5$ (1.1 − 2.0), and the flux of the PWN is $\sim 1.6 \times 10^{-12}$ erg cm^{-2} s^{-1}. The flux ratio between PSR J1838−0655 and its PWN is >5.3 in our calculation, and this ratio is at the high end of the distribution of PWNe observed by *Chandra* (Kargaltsev & Pavlov 2008). This suggests that the observed pointed-source spectrum of *Chandra* is mainly from the pulsar even if we do not have an appropriate time selection. This suggests that the unappropriate time selection cannot be the cause of the different photon indices between *RXTE* and *Chandra* spectra. The origin of the difference is still unclear; but since the *Chandra* and *RXTE* observations were carried out at different epochs, the difference might indicate that the photon index could vary with time if the difference is not caused by the uncertainty of the response functions between the different instruments.

A very interesting new discovery from the *Suzaku* observations is a marginal line feature close to 6.4 keV detected in the XIS spectra of 3 × 3 mode (Fig. 3). This line feature is only detectable in the FI detectors (XIS 0 and XIS 3) and cannot be seen in the spectrum of the BI detector (XIS 1); this might be caused by the fact that the effective area of the BI chip above 4 keV is smaller than that of the FI chips, and thus the XIS 1 is much less efficient in detecting line emission at higher energy. Detailed analysis show that this line feature is at around 6.65 keV (EW $= 150^{+300}_{-120}$ eV) and has a significance of $\sim 4\sigma$. This line feature might be the Kα emission of highly ionized Fe. We do not find similar emission feature in the spectra of the surrounding background. This excludes the possibility that this line feature may be caused by the background contamination, such as

the intense diffuse galactic ridge emission. This line feature might be originated from the surrounding ionized gas of the pulsar.

4 DISCUSSION

We have presented the results of temporal and spectral analyses for the X-ray emission from PSR J1838−0655 observed by *Chandra*, *RXTE* and *Suzaku*. According to Fig. 1, the structure of the pulse profile of *Suzaku*/PIN observation is very similar to that of *RXTE*/PCA. There is some dissimilarity of the pulse profile derived by Anada et al. (2009) and ours. This may be caused by the different selection of the zero epoch and the phase bins. We also divided the photons of *RXTE* observations into 2–10 and 10–20 keV to plot the folded light curves (shown in Fig. 4), and we did not find obvious difference from the profile structures.

Our spectral analysis indicates that there is a spectral break in the X-ray spectra of the pulsar. This might be similar to the spectral break discovered in the Crab pulsar (Kuiper et al. 2001). With non-thermal emission model, the best-fitting photon indices are $\Gamma_1 \sim 1$ and $\Gamma_2 \sim 1.5$ with a break energy $E_c \sim 6.5$ keV and with the flux of $f \sim 1.6 \times 10^{-11}$ erg cm^{-2} s^{-1} in 2–20 keV. The results provide more complete information of the spectral behaviour in addition to the studies done by Gotthelf & Halpern (2008) and by Anada et al. (2009). At a distance of $d \sim 6.6$ kpc, the efficiency of the energy conversion from the spin-down luminosity, $L_p = 5.5 \times 10^{36}$ erg s^{-1}, to the X-ray emissions is about 0.9 per cent, where we have used $L_{0.8-10\,\mathrm{keV}} \sim 5.0 \times 10^{34}$ erg s^{-1} estimated from our data analysis.

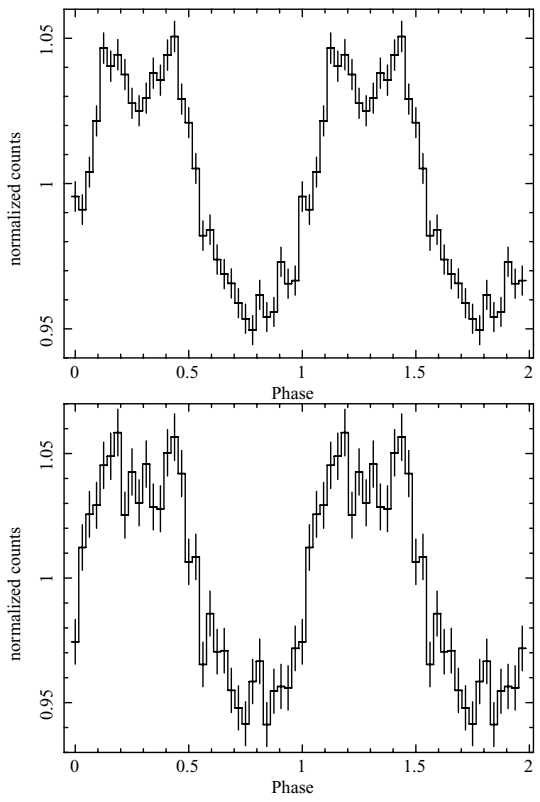

Figure 4. Pulse profile of *RXTE*/PCA observations folded at different energy bands. All the input parameters are corresponding to Fig. 1. The upper panel shows the folded light curve of PSR J1838−0655 at 2–10 keV with ∼70.5 ms and the lower panel shows similar folded profile for the same pulsar at 10–20 keV with the same period. The plot of the counts are also normalized to the average photons in each bin.

If the observed X-ray emission is caused by a non-thermal process, the emission might come from the magnetosphere around a particle acceleration region, which is called a 'gap'. Comparing the efficiency of the energy conversion from the spin-down energy to the non-thermal X-ray emission with other known non-thermal X-ray emitting pulsars listed in tables 1 and 2 of Kargaltsev & Pavlov (2008), we find that the efficiency of PSR J1838−0655, which was listed in table 3 of Kargaltsev & Pavlov (2008) for pulsars without known periods, is the third largest and is larger than that of the Crab pulsar. One might expect that the energy-conversion efficiency of PSR J1838−0655 should be similar to that of the γ-ray pulsars, PSRs B0833–44 (the Vela) and B1706–44, because these three pulsars have similar pulsar properties (e.g. the rotation periods and the surface magnetic fields). However, the efficiencies of the Vela pulsar and PSR B1706–44 are about 5×10^{-4} per cent and 3×10^{-3} per cent, respectively, and are much smaller than that of PSR J1838−0655. In fact, the efficiency of PSR J1838−0655 is in the range of younger γ-ray pulsars, such as the Crab pulsar and PSR B1509–58, which have $L_{0.8-10\,\mathrm{keV}}/L_p \sim 0.34$ per cent, and ∼0.61 per cent, respectively. Therefore, PSR J1838−0655 provides a unique opportunity to investigate the non-thermal emitting process in the pulsar magnetosphere and the connection between the X-ray and γ-ray emission.

According to the outer magnetospheric-emission model (Cheng, Ruderman & Zhang 2000), the high efficiency of the Crab pulsar can be explained as a result of the X-ray photons emitted via the synchrotron radiation of the secondary electrons and positrons produced in the pair-creation process of the primary γ-rays, which are produced in the gap. In the gap of the Crab pulsar, about 1 per cent of the spin-down energy is converted to the γ-ray emission. Considering the optical depth of the pair creation of the γ-rays using the X-ray photon number density outside the gap inferred from the Crab observations, we find that most of the primary γ-ray photons above 1 GeV are absorbed by the background X-ray photons before escaping from the magnetosphere (Fig. 5). Because there are abundant new-born electron–positron pairs, which will emit X-ray photons via the synchrotron radiation, the X-ray emission will dominate the observed energy spectral distribution of the Crab pulsar and the resultant conversion efficiency in the X-ray bands can be as large as a few point per cent.

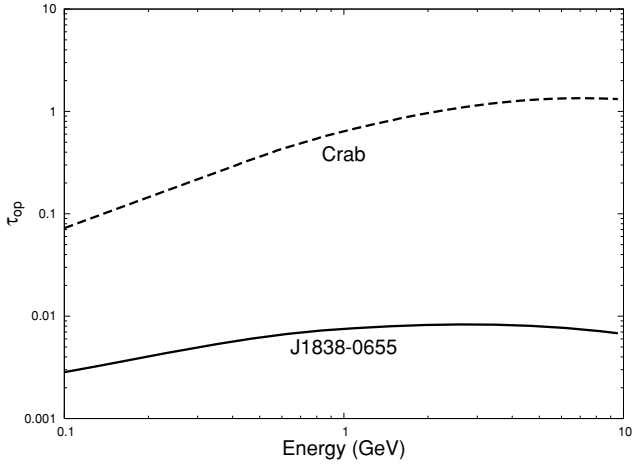

Figure 5. Optical depths from the pair creation of the γ-ray photons as a function of energy. The solid line and the dashed line represent the optical depths for PSR J1838−0655 and the Crab pulsar, respectively.

The above emission model predicts the photon indices to be $\Gamma_1 \sim 1.5$ and $\Gamma_2 \sim 2$ with a break at $E_c \sim 10$ keV (Takata, Chang & Cheng 2007). Roughly speaking, the predicted spectral property is also similar to the observed properties of the X-ray emission of PSR J1838−0655, which shows a spectral break around 6.5 keV and has a high energy conversion efficiency. However, we find that the X-ray emission model for the Crab pulsar cannot be applied to the case of PSR J1838−0655 because the optical depth of the pair creation from the γ-rays is much smaller than unity. Using the observed X-ray properties in this study, the energy distribution of the X-ray photon number density in the magnetosphere of PSR J1838−0655 is

$$\frac{\mathrm{d}N}{\mathrm{d}E_{\rm X}} = 2.8\times10^{22} d^2_{6.6\,\rm kpc}\,\mathrm{cm}^{-3}\,\mathrm{erg}^{-1} \begin{cases} (E_{\rm X}/6.5\,\mathrm{keV})^{-1}, \\ \quad \text{for } E_{\rm X} \le 6.5\,\mathrm{keV} \\ (E_{\rm X}/6.5\,\mathrm{keV})^{-1.5}, \\ \quad \text{for } E_{\rm X} > 6.5\,\mathrm{keV}. \end{cases} \quad (1)$$

We have used $\frac{\mathrm{d}N}{\mathrm{d}E_{\rm X}} = \frac{4\pi d^2}{c}\frac{\mathrm{d}n}{\mathrm{d}E_{\rm X}}\left(\frac{R_{\rm lc}}{2}\right)^{-2}$, where $\frac{\mathrm{d}n}{\mathrm{d}E_{\rm X}}$ is the observed number flux obtained in this paper and $R_{\rm lc}$ is the light cylinder. Fig. 5 compares the optical depths of the pair creation for the γ-ray photons of the PSR J1838−0655 (solid line) and of the Crab pulsar (dashed line) before escaping the magnetosphere. We see that the optical depth is much smaller than unity for the GeV γ-ray photons emitted in the gap of PSR J1838−0655, while it is about unity for those of the Crab pulsar. So the absorption of the γ-ray photons in the magnetosphere of PSR J1838−0655 is very weak, and only a few secondary pairs are created by the pair-creation process with the background X-ray fields. As a result, the synchrotron emission of the secondary pairs will not be able to explain the flux of the observed X-ray emission. On this ground, we conclude that the X-ray emission mechanism of the Crab pulsar cannot apply to PSR J1838−0655, although the energy-conversion efficiencies of both sources are similar.

A greatly inclined rotator, with the inclination angle $\alpha \sim 90^\circ$, is another possibility to explain the high energy conversion in the X-ray emission of PSR J1838−0655 and the different efficiencies between PSR J1838−0655 and the Vela pulsar. With the outer magnetospheric model, the X-ray emission from the Vela pulsar can be explained by the synchrotron emission of the secondary pairs. The secondary pairs are produced by the pair-creation process between the γ-rays and the background X-ray field and/or by the magnetic pair creation of the inwardly propagating γ-rays, which pass through the region near the stellar surface. The outer magnetospheric-emission model studied by Zhang & Jiang (2006) argued that the efficiency of the X-ray emission increases with the inclination angle. This is caused by the fact that (i) the strong acceleration of the outer gap model extends between the null charge surface of the Goldreich–Julian charge density and the light cylinder and (ii) the null charge surface shifts towards the stellar surface with increasing inclination angles from 0° to 90°. For the greater inclined rotator, therefore, more γ-rays emitted inward directions pass through vicinity of the stellar surface and are absorbed by the strong magnetic field around the stellar surface. The created secondary pairs can emit X-ray photons via the synchrotron radiation.

The magnetic pair-creation condition for a photon with energy E_γ may be written as $(\frac{E_\gamma}{m_e c^2})\frac{B}{B_c}\sin\theta_b \sim 0.2$ (Muslimov & Harding 2003), where $B_c = 4.413\times10^{13}$ G and θ_b is the angle between the magnetic-field lines and the propagating direction of γ-rays. Most of the pairs in the gap are created around the null charge surface (Takata, Shibata & Hirotani 2004). The distance from the stellar surface to the null charge surface of the last-open field line is typically $r_{\rm n} \sim \frac{R_{\rm lc}}{\sin^2(\theta_{\rm n}-\alpha)}\sin^2(\theta_{\rm lc}-\alpha)\sin\theta_{\rm lc}$, where $\tan\theta_{\rm n} = \frac{(3\tan\alpha+\sqrt{9\tan^2\alpha+8})}{2}$ and $\tan\theta_{\rm lc} = -\frac{(3+\sqrt{9+8\tan^2\alpha})}{4}\tan\alpha$ with $\theta_{\rm n}$ being the angle of the null charge surface measured from the north pole and $\theta_{\rm lc}$ being the angle to the point at which the last-open field line is tangent to the light cylinder. If we use the radial distance $r_{\rm n}$ as the emission point, the closest distance from the stellar surface to the trajectory of the inwardly propagating γ-rays emitted on the null charge surface is $r_{\rm min} \sim r_{\rm n}\sin\theta_p$, where θ_p is the angle of the null charge surface measured from rotation axis. If we estimate the minimum inclination angle, above which most of the 1 GeV γ-rays are absorbed by the strong magnetic field, with the magnetic pair-creation condition, we find that $\alpha > 60^\circ$. In reality, the pairs are created above the last-open field lines; for example, if we set the emission point with $2r_{\rm n}$, we would obtain $\alpha > 70^\circ$.

The absorbed γ-ray photons are converted into electron–positron pairs. The new-born pairs lose their energy rapidly via the synchrotron radiation; and the synchrotron photons would be converted into electron–positron pairs via the magnetic pair-creation process, if their energies are large enough for the magnetic pair-creation process. The typical energy of the synchrotron photons emitted by the first pairs is $E_1 \sim 0.075E_\gamma$, where E_γ is the energy of γ-ray photons. The typical energy of the synchrotron photons emitted by the ith generated pair can be written as $E_i \sim (0.075)^i E_\gamma$.

If the magnetic fields on the path of the photons are strong enough, the pair-creation cascade will continue until the typical energy of the synchrotron photons becomes about 1 MeV. Let us take the inclination angle of 80° and a dipole magnetic field as an example. The radial distance to the null charge surface on the last-open field line in the magnetic meridional plane is $r_{\rm n} \sim 0.028R_{\rm lc}$ (Fig. 6). We compute the pair-creation cascade initiated by 1 GeV photons emitted inwardly along the magnetic-field line at the radial distance $r \sim 0.055R_{\rm lc}$ and on the null charge surface in the magnetic meridional plane. As summarized in Fig. 6, the first pair creation occurs at $r = 0.014R_{\rm lc}$ and the typical energy of synchrotron photons

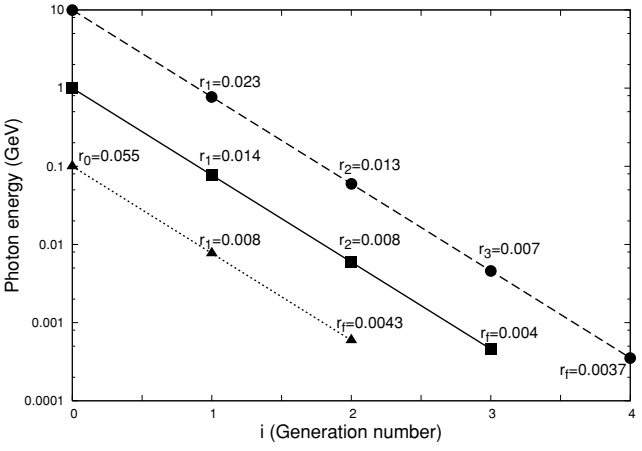

Figure 6. Cascade of the magnetic pair-creation process. The vertical axis represents the energy of the emitted photons, and the abscissa axis represents the generation number. The dashed, solid and dotted lines represent the pair cascade initiated by the photons with 10, 1 and 0.1 GeV, respectively, emitted inwardly at the radial distance $r_0 = 0.055$ in units of the light radius. The photon energies of the generation number i represent the typical energy of the synchrotron photons, and the values of r_i in the figure represent the radial distances to the pair-creation positions of ith generation.

emitted by the first generated pairs can be written as $E_1 \sim 75$ MeV. The sequence of the pair-creation cascade stops after producing the third-generation pairs at $r_f \sim 0.004 R_{\rm lc}$. The third-generation pairs are produced with a Lorentz factor of $\gamma \sim 6$ and emit synchrotron photons of ∼500 keV. The spectrum of the emission from the pairs extends with a photon index of $1.5 - 2$ (Cheng & Zhang 1996) from ∼500 keV to a break energy $E_m \sim 14$ keV, which is the characteristic energy of the synchrotron photons from the electrons/positrons with a Lorentz factor $\gamma = 1/\sin\theta_b \sim 1$. Below the break energy, the spectrum will has a photon index of $\Gamma \sim 2/3$, which represents the spectral slope of the synchrotron radiation below its characteristic energy. We find this model can explain the observed properties in the X-ray spectra of PSR J1838−0655.

Therefore, if the X-rays from PSR J1838−0655 are emitted in the magnetosphere, an inclination angle close to $\alpha \sim 90^\circ$ would be preferred in order to explain the energy-conversion rate at X-ray bands. For the Vela pulsar, the energy-conversion rate can also be explained by $\alpha = 30^\circ$ with the magnetic pair-cascade model (Zhang & Jiang 2006). On this ground, it is possible to explain the difference of the energy-conversion efficiencies of the Vela pulsar and PSR B1838–0655 by the difference of the inclination angles. The greatly inclined rotator model may also predict the absence of the radio detection. The copious pairs produced by the magnetic pair creation near the pulsar can easily supply the Goldreich–Julian number density. Therefore, if the magnetic pair-creation cascade initiated by the γ-ray from the outer gap develops in the polar cap accelerator, the electric field parallel to the magnetic field in the polar cap accelerator will be screened by the new-born pairs, indicating no coherent radio emission in the magnetosphere.

We note that most of γ-ray photons emitted outwards can escape from the magnetosphere without pair creations. The outwardly migrating particles are accelerated using a full potential drop along the field line before escaping the gap from the outer boundary located around the light cylinder; on the other hand, the inwardly migrating particles are accelerated with a small part of the potential drop between the inner boundary and the pair-creation position around the null charge surface. This implies the luminosity of the outward γ-rays is one or two order larger than that of the inward γ-rays. If the observed X-rays are originated from the inward γ-rays, the outward γ-rays would be observed with a flux similar to or greater than the X-ray flux, which is $f_{\rm X} \sim 10^{-11}$ erg cm^{-2} s^{-1}. However, we note that the observed γ-ray flux also depends on the viewing angle of the observers. Therefore, future *Fermi* observations could thus provide more information necessary to investigate the X-ray emission process with a greatly inclined rotator model.

5 CONCLUSIONS

We have reanalysed the X-ray data of *Chandra*, *RXTE* and *Suzaku* to investigate the possible X-ray emission mechanism for the X-ray pulsar PSR J1838−0655. We find that a broken power law with the photon index varying from 1.0 to 1.5 and with a break energy of ∼6.5 keV can provide a good fit for the composite X-ray spectrum. According to our results, we also found no significant energy dependence of the pulse profiles.

We have discovered a marginal Fe Kα line feature in the *Suzaku*/XIS data of PSR J1838−0655. A similar line feature was also detected in the radio pulsar PSR J1420–6048/AX J1420.1–6049 (Roberts, Romani & Johnston 2001) in *ASCA* observations. Both pulsars are found to be associated with high-energy TeV sources (i.e. HESS J1420–607 for PSR J1420–6048; Aharonian et al. 2006a); however, PSR J1420–6048 has not only a radio counterpart but also a 100-MeV γ-ray one (3EG J1420–6048). These results might indicate that the Fe Kα emission is associated with the TeV sources; however, the relation between the line emission and the TeV sources is still not clear.

We have proposed and investigated the possible mechanism for the observed X-ray emission of PSR J1838−0655. The model for a greatly inclined rotator is the most plausible scenario to explain the high efficiency- of the energy conversion from the spin-down luminosity to X-ray emission. However, it is expected to accompany with some level of γ-ray radiation. Because no unidentified Energetic Gamma-Ray Experiment Telescope (EGRET) source exists in the region around PSR J1838−0655, it requires a deeper observation in the γ-ray bands (e.g. *Fermi* telescope) to solve the mystery of the X-ray emission from this pulsar. This will also provide important clues to understand how the X-rays and the γ-rays in the magnetosphere of PSR J1838−0655 are connected.

ACKNOWLEDGMENTS

The authors thank an anonymous referee for his/her helpful comments. We also thank Dr. Albert Kong for the careful review of the manuscript and thank Drs. Hsiang-Kuang Chang, Kwong-Sang Cheng and Ronald Taam for fruitful discussion. This research has made use of the data obtained through the High Energy Astrophysics Science Archive Research Center Online Service, provided by the NASA/Goddard Space Flight Center. This work was partially supported by the National Science Council through grants NSC 98-2811-M-008-044. CYH acknowledges support from the National Science Council through grants NSC 96-2112-M-008-017-MY3 and NSC 95-2923-M-008-001-MY3. JT was supported by the Theoretical Institute for Advanced Research in Astrophysics (TIARA), operated under Academia Sinica and the National Science Council Excellence Projects program in Taiwan through grant NSC 96-2752-M-007-007-PAE.

REFERENCES

Abdo A. A., 2009, ApJ, 183, 46
Aharonian F. et al., 2005, Sci, 307, 1938
Aharonian F. et al., 2006a, A&A, 456, 245
Aharonian F. et al., 2006b, ApJ, 636, 777
Anada T., Ebisawa K., Dotani T., Bamba A., 2009, PASJ, 61, 183
Bamba A., Ueno M., Koyama K., Yamauchi S., 2003, ApJ, 589, 253
Bassani L. et al., 2004, The Astronomer's Telegram, 232, 1
Bird A. J. et al., 2004, ApJ, 607, L33
Cheng K. S., Ruderman M., Zhang L., 2000, ApJ, 537, 964
Gotthelf E. V., Halpern J. P., 2008, ApJ, 681, 515
Hartman R. C. E., 1999, ApJS, 123, 79
Hertz P., Grindlay J. E., 1988, AJ, 96, 233
Kargaltsev O., Pavlov G. G., 2008, in Bassa C., Wang Z., Cumming A., Kaspi V. M., eds, AIP Conf. Ser. Vol. 983, 40 Years of Pulsars: Millisecond Pulsars, Magnetars and More. Am. Inst. Phys., New York, p. 171
Kuiper L., Hermsen W., Cusumano G., Diehl R., Schönfelder V., Strong A., Bennett K., McConnell M. L., 2001, A&A, 378, 918
Landi R. et al., 2006, ApJ, 651, 190
Malizia A. et al., 2004, in Schoenfelder V., Lichti G., Winkler C., eds, ESA SP-552, 5th INTEGRAL Workshop on the INTEGRAL Universe. ESA, Noordwijk, p. 161
Malizia A. et al., 2005, ApJ, 630, L157

Muslimov A. G., Harding A. K., 2003, ApJ, 588, 430
Roberts M. S. E., Romani R. W., Johnston S., 2001, ApJ, 561, L187
Sugizaki M., Mitsuda K., Kaneda H., Matsuzaki K., Yamauchi S., Koyama K., 2001, ApJS, 134, 77
Takata J., Shibata S., Hirotani K., 2004, MNRAS, 354, 1120
Takata J., Chang H.-K., Cheng K. S., 2007, ApJ, 656, 1044
Warwick R. S., Norton A. J., Turner M. J. L., Watson M. G., Willingale R., 1988, MNRAS, 232, 551
Zhang L., Jiang Z. J., 2006, A&A, 454, 537

This paper has been typeset from a TEX/LATEX file prepared by the author.